

DNAct: Diffusion Guided Multi-Task 3D Policy Learning

Ge Yan*, Yueh-Hua Wu*, and Xiaolong Wang
UC San Diego

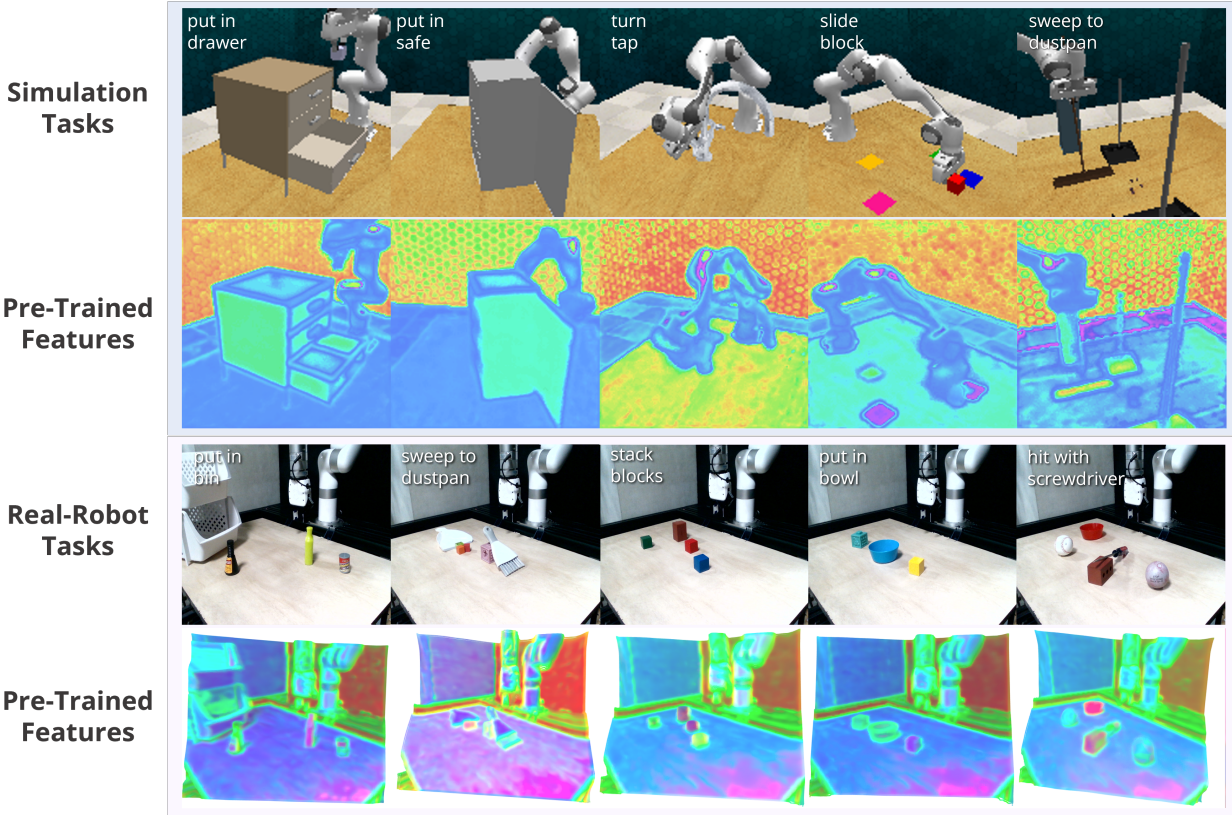


Fig. 1: We propose **DNAct**, a novel multi-task object manipulation approach that utilizes knowledge distillation and diffusion training to obtain semantic-aware and multi-modal representations. We visualize our pre-trained semantic-aware representations, demonstrating that they accurately capture the semantics in both simulated and real-world tasks by leveraging neural rendering for pre-training.

Abstract—This paper presents DNAct, a language-conditioned multi-task policy framework that integrates neural rendering pre-training and diffusion training to enforce multi-modality learning in action sequence spaces. To learn a generalizable multi-task policy with few demonstrations, the pre-training phase of DNAct leverages neural rendering to distill 2D semantic features from foundation models such as Stable Diffusion to a 3D space, which provides a comprehensive semantic understanding regarding the scene. Consequently, it allows various applications to challenging robotic tasks requiring rich 3D semantics and accurate geometry. Furthermore, we introduce a novel approach utilizing diffusion training to learn a vision and language feature that encapsulates the inherent multi-modality in the multi-task demonstrations. By reconstructing the action sequences from different tasks via the diffusion process, the model is capable of distinguishing different modalities and thus improving the robustness and the generalizability of the learned representation. DNAct significantly surpasses SOTA NeRF-based multi-task manipulation approaches with over 30% improvement in success rate. Project website: dnact.github.io.

I. INTRODUCTION

Learning to perform multi-task robotic manipulation in complex environments is a promising direction for future applications, including household robots. Recent studies have showcased the potential of this approach [44], demonstrating the possibility of training a single model capable of accomplishing multiple tasks. However, there are still significant issues to overcome. (i) To learn a generalizable multi-task policy from scratch, large-scale datasets are required for comprehensive 3D semantic understanding, which poses a challenge for real-world situations where only a small number of demonstrations are present. (ii) To learn a reliable policy that is capable of executing manipulation in complex environments, the ability to identify the multi-modality of trajectories from the given demonstrations is required. For example, considering the case where the demonstrations contain several possible trajectories avoiding cluttered objects in the kitchen to pick up a knife, a policy learning approach without handling the multi-modality

*Equal Contribution

may be biased toward one of the modes (trajectories) and fail to generalize to novel objects or arrangements.

To tackle complex tasks in a more challenging environment (*e.g.*, partial occlusion, various object shapes, and spatial relationship), it is essential to have a comprehensive geometry understanding of the scene. To achieve this, recent work [9] reconstructs a 3D scene representation by rendering with Neural Radiance Fields (NeRFs) [28]. Despite its success in single-task settings like hanging mugs requiring accurate geometry, it requires segmentation of individual objects and lacks semantic understanding of the whole scene, which makes it impractical in more complex environments. On the other hand, to learn the inherent multi-modality in the given demonstrations, previous works [8, 51] adopts diffusion models [11, 46] to learn an expressive generative policy that possesses the potential to identify different modes, which in turns elevates its success rate. However, in these studies, only relatively simple tasks such as single-task learning are considered. We further observe that in our experiments where the agent is required to perform multi-task manipulation, it is very challenging to leverage diffusion policies to predict accurate action sequences and substantial parameter tuning may be required for more complex tasks. Additionally, the extensive inference time of diffusion models is a significant drawback, preventing their application to real robots and complex tasks that require both accuracy and swift inference.

To address these challenges, we learn a unified 3D representation by integrating neural rendering pre-training and diffusion training. Specifically, we first pre-train a 3D encoder via neural rendering with NeRF. We not only utilize the neural rendering to synthesize novel views in RGB but also predict the corresponding semantic features from 2D foundation models. From distilling pre-trained 2D foundation models, we learn a generalizable 3D representation with commonsense priors from internet-scale datasets. We show that this pre-training representation equips the policy with out-of-distribution generalization ability.

Differing from previous work [41], our method presents no requirement for task-specific in-domain data for 3D pre-training. To optimize the model to distinguish multi-modality as well as similarity from the multi-task demonstrations as suggested in Figure 2, we perform diffusion training to supervise the representation. The diffusion training of DNAAct involves the optimization of a feature-conditioned noise predictor and the predictor is designed to reconstruct action sequences across different tasks. With the reconstruction process, the model can effectively identify the inherent multi-modality in the trajectories without biasing toward a certain mode. The learned policy is able to achieve a higher success rate not only in the training environments but also in the environments where novel objects and arrangement is present due to the structured and generalizable representation optimized by the diffusion training. Figure 3 summarizes the concept proposed in DNAAct. It illustrates that the 3D semantic feature is learned at the pre-training phase by reconstructing RGB and the corresponding 2D semantic features. In addition, the proposed diffusion training

further enhances the ability to discriminate various modes arising from different tasks.

Our contributions are summarized below:

- 1) We utilize NeRF for 3D pre-training to learn a unified semantic and geometric representation. By distilling pre-trained 2D foundation models into 3D space, we generate a 3D semantic representation enriched with commonsense priors from large-scale datasets, demonstrating strong out-of-distribution generalization. Unlike other NeRF-based methods [9, 57, 23], our approach does not require costly, task-specific in-domain datasets of multi-view images and action data for 3D pre-training.
- 2) DNAAct employs diffusion training to distinguish features across multi-modal, multi-task demonstrations. It leverages a feature-conditioned noise predictor and a diffusion process to distinguish modalities, enhancing the robustness and generalizability of our representation. The integrated policy network simplifies the learning process, bypassing the extensive denoising phase and stabilizing multi-task learning.
- 3) DNAAct achieves a **1.35x** improvement in simulation and a **1.33x** improvement in real-world robot experiments with only 30% of the parameters required by baseline methods. Remarkably, DNAAct surpasses baselines by **1.25x**, even when pre-trained on orthogonal tasks unrelated to subsequent training and evaluation. In scenarios with novel objects, our ablation study shows DNAAct outperforming baselines by **1.70x**.

II. RELATED WORK

Multi-Task Robotic Manipulation Recent advancements in multi-task robotic manipulation are making significant improvements in performing complex tasks and adapting to new scenarios [38, 16, 3, 42, 55, 54]. Many standout methods generally use extensive interaction data to develop multi-task models [16, 3, 42, 20]. For instance, RT-1 and RT-2 [3, 4] have demonstrated improved performance in real-world robotic tasks across various datasets.

To mitigate the need for extensive demonstrations, techniques that use keyframes have been shown effective [47, 30, 29, 53, 22, 57]. PerAct [43] incorporates the Perceiver Transformer [13] to understand language goals and voxel observations, proving its value in real-world robot experiments. In our study, we are using the same action prediction model as PerAct, but we are focusing on increasing the model’s ability to generalize by learning a generalized and multimodal representation with limited data.

3D Representations for Policy Learning.

To enhance manipulation policies using visual information, many studies have focused on improving 3D representations. Ze et al. [56] employ a 3D autoencoder, showing improved sample efficiency in motor control compared to 2D methods. Driess et al. [9] uses NeRF for learning state representation, demonstrating initial success but with limitations, such as the requirement for object masks and the absence of scene structure and the robot arm, affecting its real-world applicability.

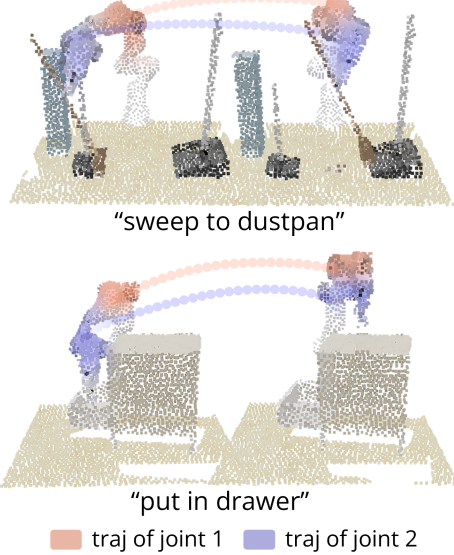


Fig. 2: **Similarity in multi-task demonstrations.** We observed that trajectories in multi-task datasets originate from varied tasks, but they exhibit similarity. This is because similar operations and sub-trajectories are often employed across different tasks.

GNFactor [57], similar to our proposed DNAAct, utilize a vision foundation model in NeRF. However, GNFactor, by jointly optimizing NeRF and behavior cloning, reduces the quality of neural rendering and limits the benefits from the semantic information. Our DNAAct addresses these challenges by learning with scene-agnostic semantic and adaptive point-cloud features in multi-task real-world scenarios, showcasing potential for real applications with a smaller number of parameters and faster inference time. In addition, DNAAct can potentially utilize widely accessible task-agnostic multi-view images such as SUN3D [52] to pre-train a versatile 3D foundation model for various downstream robotic tasks whereas GNFactor’s approach is limited in learning high-quality 3D semantics representation and difficult to scale up learning due to its requirements for task-specific multi-view images paired with action data. The proposed diffusion training for learning multi-modal representations from observations makes DNAAct a more capable approach than GNFactor, especially when learning from multi-task demonstrations where multi-modality occurs due to multiple similar trajectories.

Neural Radiance Fields. Over the years, neural fields have made significant advancements in novel view synthesis and scene representation learning [7, 27, 28, 31, 33, 45], with efforts to merge them into robotics [19, 26, 23, 9, 41]. NeRF [28] and its variants [6, 17, 25, 39, 40, 48, 50] have been remarkable for enabling photorealistic view synthesis by learning a scene’s implicit function, but its need for per-scene optimization limits its generalization.

Diffusion Models for Policy Learning. The growing interest in diffusion models [46, 11] has led to important advancements in RL and robotic learning methods. This interest is due to the success of generative modeling in tackling various decision-making problems, with applications in both policy and robotic

learning domains [18, 24, 51, 2, 5, 1, 49, 12, 8]. In robotics, [18] and [12] have explored the use of diffusion models in planning to infer possible action trajectories in different environments. This research aligns with works like [10] reinterpreting Implicit Q-learning using diffusion parameterized behavior policies. Unlike these methods, the proposed DNAAct doesn’t directly use diffusion models for action inference but uses them to derive multi-modal representation and jointly optimize a policy network, offering more stable training and eliminating the need for the costly inference of diffusion models.

III. METHOD

In this section, we elaborate on our proposed method, DNAAct. The DNAAct learns a language-conditioned multi-task policy by leveraging a pre-trained 3D encoder from neural rendering. The 3D encoder is then frozen and paired with a point-cloud encoder, which is trained from scratch. Together, they work to predict representations of observations that preserve the multi-modality within the trajectories, utilizing a diffusion training approach.

A. Robotic Manipulation as Keyframe Prediction

Given the computational demands and data inefficiency inherent in continuous action prediction, we reformulate the problem of learning from demonstrations in robotic manipulation as a keyframe-prediction problem [43, 15]. Keyframes are identified from expert demonstrations using a specific metric: a frame is considered a keyframe if the joint velocities approach zero and the gripper maintains a consistent open state. Subsequently, the model is trained to predict the subsequent keyframe based on the current point-cloud observations. This keyframe-prediction problem retains a similarity to the original learning from demonstrations in terms of the training procedure whereas to represent the action of the robot arm with a gripper, we estimate the translation $a_{\text{trans}} \in \mathbf{R}^3$, rotation $a_{\text{rot}} \in \mathbf{R}^{(360/5) \times 3}$, gripper openness $a_{\text{open}} \in [0, 1]$, and collision avoidance $a_{\text{collision}} \in [0, 1]$. The rotation action is discretized into 72 bins for 5 degrees each bin per rotation axis, and the collision avoidance indicator $a_{\text{collision}}$ estimates the need for contact. This approach effectively transforms the computationally intensive continuous control problem into a more manageable, discretized keyframe-prediction task, allowing the motion planner to handle the intricate procedures.

B. 3D Encoder Pre-Training with Neural Feature Fields

To develop a scene-agnostic 3D encoder capable of providing comprehensive 3D semantic information of complex environments, we leverage neural rendering and knowledge distillation for 3D encoder pre-training. This method constructs 3D semantics from a 2D foundational model through neural rendering with NeRF. With higher sample efficiency, this pre-training paradigm significantly facilitates training efficiency and model performance across various task domains.

When learning from a limited set of demonstrations, our method of pre-training and subsequently using the frozen 3D

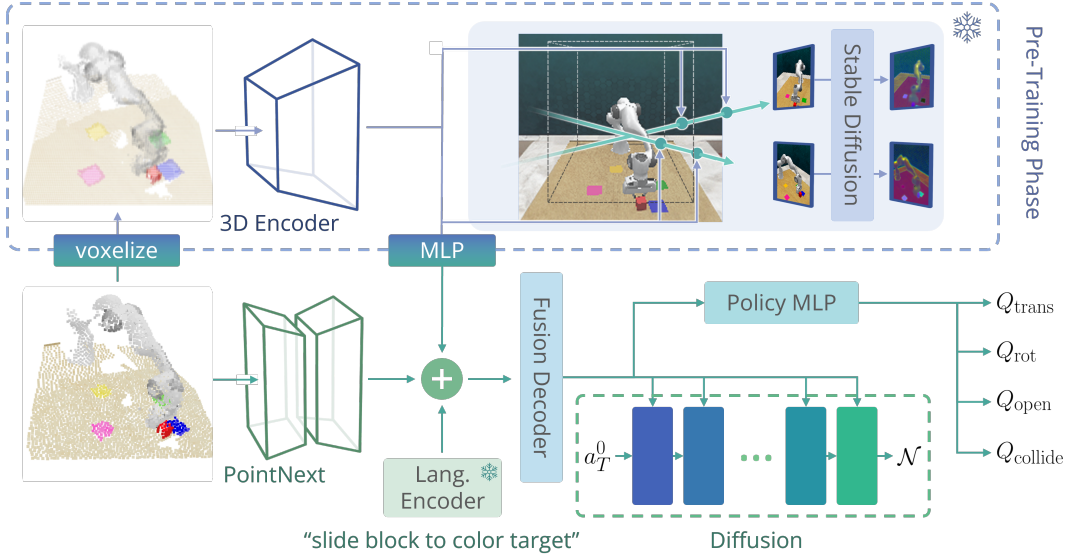


Fig. 3: The diagram provides an overview of the proposed DNAAct. The upper section of the figure represents the pre-training component, which is frozen during the subsequent training phase, as indicated by the snowflake icon. The area shaded in gray does not participate in this training phase, with only the 3D encoder being utilized to provide generic semantic features. The lower section of the figure corresponds to the training phase, where the diffusion training and the policy MLP are jointly optimized. a_0^T suggests an action sequence of length T and \mathcal{N} is the normal distribution.

encoder for downstream tasks ensures that the subsequent decision-making process leverages accurate 3D semantics rather than overfitting to the demonstrations with behavior cloning. Additionally, the pre-training does not necessitate paired action in the training dataset, expanding the possibility of utilizing a broader range of training datasets unrelated to the target tasks and scenes directly. This approach eliminates the need for task-specific data in both NeRF and policy training, enhancing scalability and versatility.

Firstly, we convert point-cloud observations into a 100^3 voxel. Our 3D encoder then encodes the voxel into a volume feature, denoted as $v \in \mathbb{R}^{100^3 \times 64}$. We then sample point feature $v_x \in \mathbb{R}^{64}$ from the volume feature by employing a trilinear interpolation operation to approximate v_x over a discrete grid in 3D space. Three distinct functions are further utilized for volumetric rendering of novel views and corresponding vision-language features:

- 1) A density function $\sigma(x, v_x) : \mathbb{R}^{3+64} \mapsto \mathbb{R}_+$, mapping the 3D point x and the 3D feature v_x to density σ .
- 2) An RGB function $c(x, d, v_x) : \mathbb{R}^{3+3+64} \mapsto \mathbb{R}^3$, assigning color to the 3D point x , the view direction d , and the 3D feature v_x .
- 3) A vision-language embedding function $f(x, d, v_x) : \mathbb{R}^{3+3+64} \mapsto \mathbb{R}^{512}$, correlating the 3D point x , the view direction d , and the 3D feature v_x to the vision-language embedding.

The rendered color and feature embedding are estimated through integration along the ray:

$$\begin{aligned} \hat{C}(r, v) &= \int_{t_n}^{t_f} T(t) \sigma(r(t), v_{x(t)}) c(r(t), d, v_{x(t)}) dt, \\ \hat{F}(r, v) &= \int_{t_n}^{t_f} T(t) \sigma(r(t), v_{x(t)}) f(r(t), d, v_{x(t)}) dt, \end{aligned} \quad (1)$$

where $T(t) = \exp\left(-\int_{t_n}^t \sigma(s) ds\right)$, $r(t) = \mathbf{o} + t\mathbf{d}$ represents the camera ray, $\mathbf{o} \in \mathbb{R}^3$ is the camera's origin coordinate, \mathbf{d} is the view direction, and t is depth, bounded by $[t_n, t_f]$.

Our 3D encoder is optimized by reconstructing the multi-view RGB images and vision language embedding through the following MSE loss:

$$\mathcal{L}_{\text{recon}} = \sum_{r \in \mathcal{R}} \|\mathbf{C}(r) - \hat{\mathbf{C}}(r)\|_2^2 + \lambda_{\text{feat}} \|\mathbf{F}(r) - \hat{\mathbf{F}}(r)\|_2^2, \quad (2)$$

where $\mathbf{C}(r)$ is the ground truth color, $\mathbf{F}(r)$ is the ground truth embedding generated by a vision-language foundation model. For more information about $\mathbf{F}(r)$, please refer to the Stable Diffusion Feature Extraction section in the experimental setup. \mathcal{R} represents the set of rays emanating from camera poses, and λ_{feat} is the weight attributed to the embedding reconstruction loss. Lastly, similar to the manner in which we approximate the 3D feature v_x , we utilize trilinear interpolation on the features predicted by the 3D encoder to derive the features corresponding to points in the point cloud.

C. Diffusion-Guided Feature Learning with Action Sequences

For the subsequent training phase, to facilitate the agent's utilization of pre-trained 3D semantic features and to ensure adaptability to a variety of tasks, the downstream action prediction models additionally incorporate a point-cloud feature, encoded by a PointNext network [36]. Specifically, given the pointcloud observation, we sample 4096 points as input of the PointNext to learn a geometric point features, denoted as $v_p \in \mathbb{R}^{4096 \times 32}$. The sampled points are also proceeded to query the 3D semantic features from pre-trained 3D volume feature v , denoted as $v_s \in \mathbb{R}^{4096 \times 64}$. The robot's proprioception is projected into a 32-dimensional vector by applying a linear layer, while the language goal features from CLIP are projected

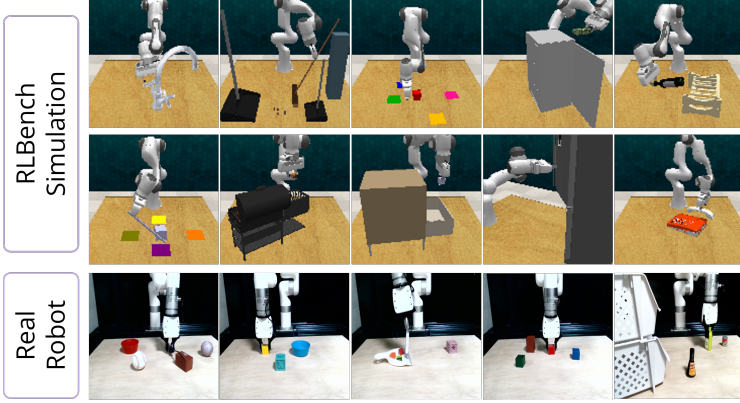


Fig. 4: The ten RLBench and five real robot tasks in our experiments.

into a 64-dimensional vector. Both vectors are then attached to each sampled point, resulting in the sequence of size 4096×32 and 4096×64 for the robot’s proprioception and language respectively. We concatenate all features together, including pre-trained semantic features v_s , point-cloud features v_p , robot proprioception, and language embeddings. This combined feature is further fused through several set abstraction layers [35] to obtain the final vision-language embedding v_f .

Through our multi-task robotic manipulation experiments, we demonstrate that learning with both the pre-trained features and the newly encoded features from PointNext offers notable generalization and an enhanced capability to capture semantic information. This underscores the effectiveness of a multi-task manipulation agent when combining insights derived from a pre-trained 3D encoder with those from a learning-from-scratch encoder.

1) *Diffusion Models as Representation Learning*: To further effectively integrate pre-trained semantic features v_s , point-cloud features v_p , and language embeddings v_l from foundation models like CLIP, we formulate the representation learning as an action sequence reconstruction problem with Denoising Diffusion Probabilistic Models (DDPMs) [11]. Learning representation with diffusion models encapsulates the multi-modality inherent in multi-task demonstrations into a fused representation.

Starting from a random action sequence a_T^K of length T sampled from Gaussian noise, the DDPM performs K iterations of denoising to produce $a_T^k, a_T^{k-1}, \dots, a_T^0$, until the action reconstruction is achieved. We perform the action denoising process with a fused feature-conditioned noise predictor via Feature-wise Linear Modulation [34]:

$$a_T^{k-1} = \alpha(a_T^k - \gamma\epsilon_\theta(v, a_T^k, k) + \mathcal{N}(0, \sigma^2 I)), \quad (3)$$

where ϵ_θ is the conditional noise prediction network parameterized by θ , v_f is the fused feature encoded by an MLP with input (v_s, v_p, v_l) , and $\mathcal{N}(0, \sigma^2 I)$ is Gaussian noise added at each iteration. The noise prediction network takes the fused feature as condition via Feature-wise Linear Modulation [34].

For each training instance, we randomly select a denoising iteration k and sample a random noise ϵ^k with a variance

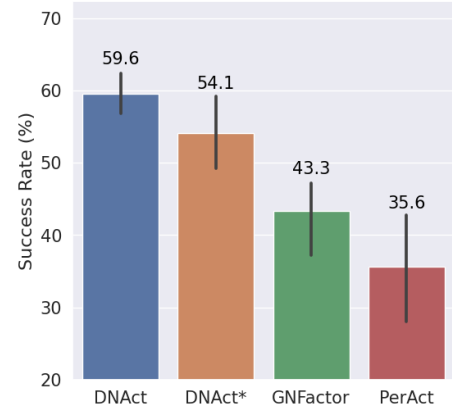


Fig. 5: Average success rates across 3 seeds on RL-Bench. The error bar shows one standard deviation.

schedule. The conditional noise prediction network is optimized to predict the noise from the data sample with noise added:

$$\mathcal{L}_{\text{diff}} = \mathbb{E}\|\epsilon^k - \epsilon_\theta(v_f, a_T^0 + \epsilon, k)\|_2^2, \quad (4)$$

where v_f is the output of the fusion decoder (Fig. 3) with concatenated v_s, v_p, v_l as inputs. The gradient from the loss function propagates through the noise decoder, the fusion decoder, and lastly the PointNext architecture. As shown in [11], minimizing the loss function (Eq. 4) essentially minimizes the variational lower bound of the KL-divergence between the data distribution and the distribution of samples drawn from the DDPM.

To predict actions for robotic manipulation, we optimize a policy network that estimates the Q-values for each action: Q_{trans} , Q_{rot} , Q_{open} , and $Q_{\text{collision}}$ corresponding to a_{trans} , a_{rot} , a_{open} , and $a_{\text{collision}}$ via behavior cloning. This policy network shares the fused feature, v_f , with the diffusion model. The objective for DNAAct at the training phase can be summarized as:

$$\mathcal{L} = \mathcal{L}_{\text{bc}} + \lambda_{\text{diff}}\mathcal{L}_{\text{diff}}, \quad (5)$$

where

$$\mathcal{L}_{\text{bc}} = -\lambda_{\text{trans}}|Q_{\text{trans}} - Y_{\text{trans}}| - \lambda_{\text{rot}}\mathbb{E}_{Y_{\text{rot}}} [\log \mathcal{V}_{\text{rot}}] - \lambda_{\text{open}}\mathbb{E}_{Y_{\text{open}}} [\log \mathcal{V}_{\text{open}}] - \lambda_{\text{collide}}\mathbb{E}_{Y_{\text{collide}}} [\log \mathcal{V}_{\text{collide}}] \quad (6)$$

$\mathcal{V}_i = \text{softmax}(\mathcal{Q}_i)$ for $\mathcal{Q}_i \in [Q_{\text{open}}, Q_{\text{rot}}, Q_{\text{collide}}]$ and $Y_i \in [Y_{\text{rot}}, Y_{\text{open}}, Y_{\text{collide}}]$ is the ground truth one-hot encoding. For translation, we calculate $L1$ loss between a predicted continuous 3D coordinate Q_{trans} and the ground truth Y_{trans} .

While using a diffusion model for action prediction with the denoised a_T^0 has been recognized for its potential to achieve state-of-the-art performance, it is empirically observed to be highly sensitive to specific architectures and configurations. For example, a balance is needed in the network architecture’s expressiveness to avoid unstable training while ensuring capability [10]. Additionally, varying configurations and hyper-parameters are required for different tasks [8], complicating the learning process for a single multi-task agent.

Consequently, we propose to learn the multi-modalities inherent in multi-task demonstrations with diffusion training.

TABLE I: **Multi-Task Performance on RL Bench.** We evaluate 25 episodes for each checkpoint on 10 tasks across 3 seeds and report the success rates (%) of the final checkpoints. Our method outperforms the most competitive baseline PerAct [43] and GNFactor [57] with an average improvement of **1.67x** and **1.38x**

Methods	turn tap	drag stick	open fridge	put in drawer	sweep to dustpan	meat off grill	phone on base	place wine	slide block	put in safe	Average
PerAct	57.3 \pm 6.1	14.7 \pm 6.1	4.0 \pm 6.9	16.0 \pm 13.9	4.0 \pm 6.9	77.3 \pm 14.0	98.7\pm2.3	6.7 \pm 6.1	29.3 \pm 22.0	48.0\pm26.2	35.6
GNFactor	56.0 \pm 14.4	68.0 \pm 38.6	2.7 \pm 4.6	12.0 \pm 6.9	61.3\pm6.1	77.3 \pm 9.2	96.0 \pm 6.9	8.0 \pm 6.9	21.3 \pm 6.1	30.7 \pm 6.1	43.3
DNAAct	73.3\pm4.6	97.3\pm4.6	22.7\pm16.2	54.7\pm22.0	24.0 \pm 17.4	92.0\pm6.9	82.7 \pm 12.2	65.3\pm9.2	58.7\pm20.5	25.3 \pm 8.3	59.6

TABLE II: We also report the success rates (%) of the **best checkpoints** for each tasks across 3 seeds. Our method achieves **1.65x** and **1.30x** improvement compared with PerAct and GNFactor

Methods	turn tap	drag stick	open fridge	put in drawer	sweep to dustpan	meat off grill	phone on base	place wine	slide block	put in safe	Average
PerAct	66.7 \pm 4.6	38.7 \pm 6.1	12.0 \pm 6.9	30.7 \pm 6.1	4.0 \pm 6.9	85.3 \pm 8.3	100.0\pm0.0	13.3 \pm 2.3	38.7 \pm 6.1	62.7\pm11.5	45.2
GNFactor	73.3 \pm 6.1	92.0 \pm 8.0	17.3 \pm 6.1	26.7 \pm 12.2	68.0 \pm 8.0	81.3 \pm 8.3	100.0\pm0.0	29.3 \pm 2.3	42.7 \pm 12.2	45.3 \pm 4.6	57.6
DNAAct	85.3\pm6.1	100.0\pm0.0	28.0\pm10.6	70.7\pm12.9	86.7\pm2.3	96.0\pm4.0	89.3 \pm 6.1	72.0\pm6.9	84.0\pm8.0	34.7 \pm 6.1	74.7

TABLE III: **Generalization to unseen tasks on RL Bench.** We evaluate 25 episodes for each task with the final checkpoint across 3 seeds.

Methods	put in drawer (with distractor)	place wine (new position)	slide block (larger object)	meat off grill (new position)	put in safe (with distractor)	Average
PerAct	5.3 \pm 2.3	2.7 \pm 4.6	32.0 \pm 14.4	66.7 \pm 23.1	42.7\pm15.1	29.8
GNFactor	18.7 \pm 6.1	12.0 \pm 10.6	22.7 \pm 18.0	72.0 \pm 10.6	29.3 \pm 23.1	30.9
DNAAct	52.0\pm8.0	30.7\pm16.2	54.7\pm28.1	93.3\pm2.3	30.7 \pm 22.0	52.3

Rather than deploying the generated actions from the diffusion model for robot control during inference, we employ an additional policy network optimized jointly to predict actions using the fused feature shared with the diffusion model. Our method, with the additional policy network, has two key benefits: (i) It ensures quicker action inference as the policy network predicts actions faster than the diffusion model, which requires multiple denoising steps. (ii) The policy network compensates for the diffusion model’s limitations in action prediction accuracy, which enhances the robustness of the entire training pipeline regarding hyper-parameters and configurations.

IV. EXPERIMENTS

A. Experiment Setup

Simulation. We conduct all simulated experiments on RL-Bench [14], a challenging large-scale benchmark and learning environment for robot learning. A 7 DoF Franka Emika Panda robot arm is equipped with a parallel gripper and affixed to a table for the execution of various tasks. Visual observations are collected from four RGB-D cameras, placed at the front, left shoulder, right shoulder, and wrist with a resolution of 128 \times 128. We convert obtained RGB and depth images to point cloud using camera intrinsics. Each task has multiple variations on different aspects like shape and color with textual summarizing descriptions. We select 10 challenging language-conditioned tasks with 50 demonstrations per task for training. To succeed with limited training, the agent needs to learn generalizable manipulation skills instead of just overfitting to the training examples.

Real Robot. We set up a tabletop environment using the xArm7 robot with a parallel gripper for real robot experiments.

We design 5 tasks with distractors in the scene, including *Put in Bowel*, *Stack Blocks*, *Hit Ball*, *Put in Bin*, *Sweep to Dustpan*, as shown in the Figure 4. We place three RealSense cameras around the robot to capture multi-view images for Neural Radiance Fields training. For policy training and evaluation, we only use the front RealSense camera to obtain RGB-D images and convert them to point cloud input. Example real-robot tasks are shown in Figure 8.

Stable Diffusion Feature Extraction. We use RGB images and corresponding language instructions as input for the Stable Diffusion model. Specifically, we encode the language instruction with a pre-trained text encoder and extract the text-to-image diffusion UNet’s internal features by feeding language embedding and RGB images into the UNet without adding noise. The rich and dense diffusion features are then extracted from the last layer of the UNet blocks. We only require a single forward pass to extract visual features instead of going through the entire multi-step generative diffusion process.

Demonstration Collection. We collect 50 demonstrations for each task in the RL Bench environment using RRT-Connect [21] motion planner. For real-world experiments, we collect 10 demonstrations using Linear Motion for each task with an HTC Vive controller.

Training Details. We train DNAAct for 50K iterations with a batch size of 32 with two NVIDIA RTX3090 GPUs, taking less than 12 hours. We train PerAct and GNFactor for 200K iterations with a batch size of 2 taking over 2 and 4 days, respectively.

B. Simulation Results

Multi-Task Performance. As shown in Table I and II, DNAAct outperforms PerAct and GNFactor across various tasks,

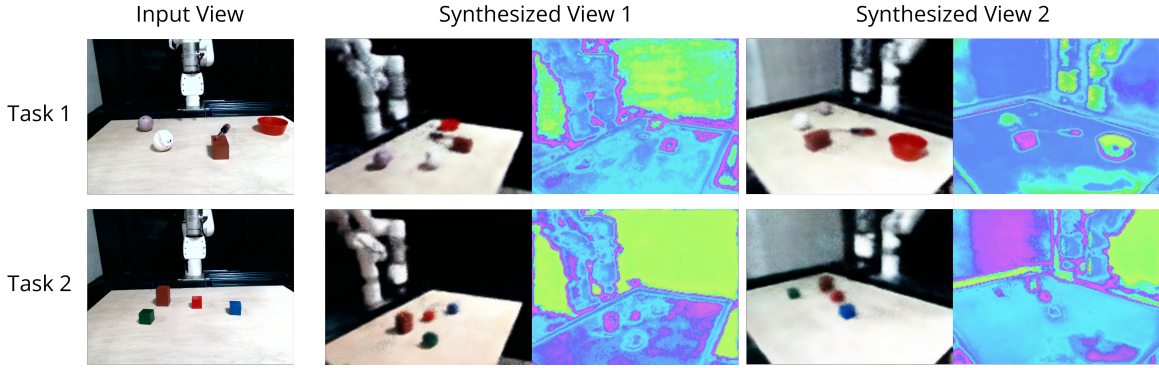


Fig. 6: **Multi-View synthesis of DNAAct in the real world.** We learn 3D semantic representations by distilling vision foundation models. The rendered feature maps are visualized on the right side.

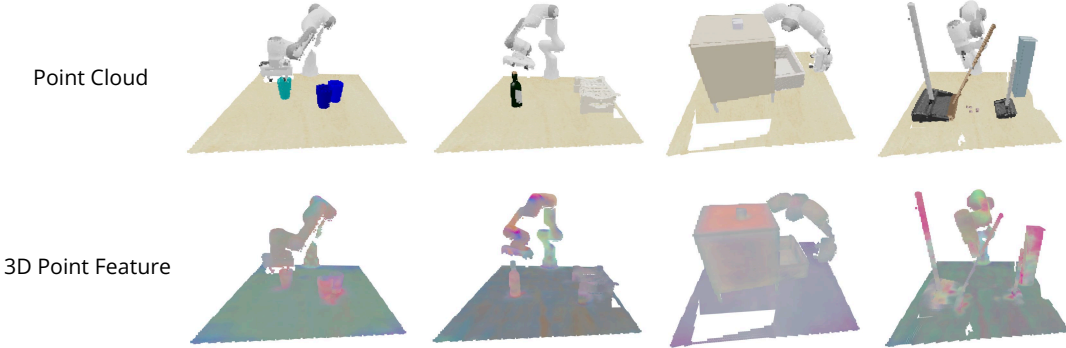


Fig. 7: **3D point features.** The visualization shows 3D point features extracted from unseen data by leveraging the pre-trained 3D encoder. We show that our model can effectively learn an accurate 3D semantic representation and generalize to out-of-domain data.

TABLE IV: An ablation study on different components of DNAAct. LfS indicates learning from scratch and Task-agnostic Pre-training suggests that a dataset from a different set of tasks are used for the pre-training phase.

Ablation	Success Rate (%)
DNAAct	59.6
LfS	33.2
w/o. Diffusion objective	51.8
Stable Diffusion → DINOv2	52.4
Stable Diffusion → CLIP	53.2
Task-agnostic Pre-training	54.1
Actions from Diffusion Model	14.2

TABLE V: Success rates (%) on real robot tasks.

Tasks	PerAct	DNAAct
Put in Bowel	40	50
Stack Blocks	40	30
Hit Ball	30	60
Put in Bin	60	80
Sweep to Dustpan	40	60
Average	42	56

especially in challenging long-horizon and fine-grained tasks. For example, in *open fridge* task, it requires the agent to have accurate 3D geometry understanding to precisely grasp the door

and open it without collisions. DNAAct can achieve a success rate of 22.7% while both PerAct and GNFActor demonstrate a minor success rate on it. For *put in drawer* task, the robot needs to first open the drawer, pick up the item, and finally put it in the drawer. It presents a comprehensive challenge to robots in long-horizon planning. We find that DNAAct achieves a 54.7% success rate, largely outperforming PerAct and GNFActor. Notably, DNAAct only uses 11.1M parameters, significantly less than PerAct (33.2M parameters) and GNFActor (41.7M parameters). These results demonstrate that DNAAct is both more efficient and capable of handling various tasks.

Generalization Performance to Unseen Tasks. The ability of a robotic agent to generalize to unseen environments with novel attributes is critical for operational versatility and adaptability. Such environments often introduce challenges, including distracting objects, larger objects, and new positional contexts. As illustrated in Table III, our proposed method, DNAAct, showcases robustness and adaptability, achieving significantly higher performance compared to the baseline methods, PerAct and GNFActor.

This superior performance of DNAAct is attributed to the 3D semantic pre-training and diffusion training. These practices allow DNAAct to optimize the learned representation from different perspectives, such as knowledge distillation and action sequence reconstruction, going beyond merely optimizing the behavior cloning objective. This prevents our model from overfitting to the training demonstrations on predicting actions.

DNAAct is particularly proficient in situations impacted by external distractors, size alterations of objects, and novel positions, maintaining high performance amidst diverse challenges. This underscores DNAAct’s superior generalization capabilities and sophisticated learning mechanism, marking it as a promising advancement in the domain of robotic manipulation.

Pre-Training on Out-of-Domain Data. Typically, NeRF-based imitation/reinforcement learning requires task-specific data for both neural rendering and policy learning. However, in the proposed DNAAct, employing pre-trained representations can enhance scalability with out-of-domain data. We delve deeper into the efficacy of DNAAct by utilizing five out-of-domain tasks, each with fifty demonstrations, to pre-train the 3D encoder via neural rendering; this variant is denoted as DNAAct*. As depicted in Figure 5, DNAAct* attains a substantially higher success rate compared to both PerAct and GNFactor and showcases performance merely slightly worse than DNAAct, which utilizes in-domain data. This underscores the significant potential of leveraging out-of-domain data for pre-training a 3D encoder through neural rendering. We hypothesize that pre-training with even larger-scale out-of-domain datasets could yield more pronounced effectiveness. We also show the visualization of the 3D point feature extracted from the pre-trained 3D encoder as in Figure 7.

Ablation. We conduct ablation experiments to analyze the impact of several key components in DNAAct. From the following experiment, we obtained several insights:

(i) Pre-trained representations via neural rendering are crucial in multi-task robot learning. As shown in table IV, a Learning-from-Scratch PointNext denoted as LfS, has a much lower success rate without fusing pre-trained 3D representations. This strongly demonstrates the efficacy of pre-training 3D representations by distilling the foundation model feature.

(ii) The ablation study reveals a 13.09% performance decrease when not learning jointly with diffusion training. This suggests that the representations optimized by the diffusion model enable the policy network to make more comprehensive decisions compared to solely optimizing the behavior cloning objective. Beyond the inherent benefits of diffusion training, the optimization of the diffusion model with action sequences potentially embeds action sequence information into the representation. This enhancement is crucial, improving the policy network, which predicts only one step at each timestep.

(iii) We further investigate the impact of different foundation models for feature distillation. By replacing the stable diffusion model with the foundation model DINOv2 [32] and vision-language foundation model CLIP [37], both models have slightly lower success rates compared with the stable diffusion model. This may be because SD features provide a higher quality spatial information. However, DNAAct with these two features still outperforms the baseline by a large margin, demonstrating the remarkable ability of foundation models.

(iv) We also report the performance by actions predicted by the diffusion model in Table IV. Utilizing diffusion models to estimate the optimal action, referred to as diffusion policy [18, 24, 51, 2, 5, 1, 49, 12, 8], has shown promise

as a policy learning model. However, we observed that the diffusion policy struggles to accurately predict keyframe actions, resulting in relatively low success rates. We attribute this issue to the discontinuity between keyframe observations and actions. The effectiveness of diffusion policy hinges on its ability to learn continuous, multi-modal trajectories. Keyframe observations and actions, while reducing the number of decisions required for complex tasks, present a challenge due to the significant differences in representation at each timestep. This makes accurate action sequence prediction difficult for sequence-based models like diffusion policy. Our proposed method, DNAAct, utilizes diffusion models from a representation learning perspective, learning multi-modal representations for observations. This approach is simple, easier to train, and can seamlessly integrate with various policy learning-based methods.

C. Real-Robot Results

We summarize the performance of DNAAct on 5 real robot tasks in table V. As shown in Figure 6, we provide the novel view synthesis results of DNAAct on both RGB and diffusion features in the real world. It shows DNAAct parses all object instances and extracts scene semantics effectively. From the experiments, DNAAct achieves an impressive average success rate of 56%, while PerAct attains 42%. Notably, in the task *Hit ball*, it requires the robot to pick the screwdriver, locate the ball, and hit it with the presence of multiple distractors. DNAAct achieves a 60% success rate in this challenging task, largely outperforming the 30% success rate of PerAct. Another example is the *Sweep to Dustpan* task, where the robot arm needs to identify the location of the debris and the dustpan, and precisely grasp the broom with complex motion. Although DNAAct demonstrates strong capability, it still lacks the ability to deal with scenes characterized by intricate spatial relationships and novel language commands. This challenge could potentially be addressed through the integration of a multi-modal large language model, leveraging its zero-shot generalization capabilities and enhanced reasoning skills to augment the performance of DNAAct.

V. CONCLUSION

In this work, we propose DNAAct, a generalized multi-task policy learning approach for robotic manipulation. DNAAct leverages a NeRF pre-training to distill 2D semantic features from foundation models to a 3D space, which provides a comprehensive semantic understanding regarding the scene. To further learn a vision and language feature that encapsulates the inherent multi-modality in the multi-task demonstrations, DNAAct is optimized to reconstructs the action sequences from different tasks via diffusion process. The proposed diffusion training at the training phase enables the model to not only distinguish representation of various modalities arising from multi-task demonstrations but also become more robust and generalizable for novel objects and arrangements. DNAAct shows promising results in both simulation and real world experiments. It outperforms baseline approaches by over 30% improvement

in 10 RLBench tasks and 5 real robot tasks, illustrating the generalizability of the proposed DNAct. **We are committed to releasing the code.**

REFERENCES

[1] Anurag Ajay, Yilun Du, Abhi Gupta, Joshua Tenenbaum, Tommi Jaakkola, and Pulkit Agrawal. Is conditional generative modeling all you need for decision-making? *arXiv preprint arXiv:2211.15657*, 2022.

[2] Arthur Argenson and Gabriel Dulac-Arnold. Model-based offline planning. *arXiv preprint arXiv:2008.05556*, 2020.

[3] Anthony Brohan, Noah Brown, Justice Carbalal, Yevgen Chebotar, Joseph Dabis, Chelsea Finn, Keerthana Gopalakrishnan, Karol Hausman, Alex Herzog, Jasmine Hsu, et al. Rt-1: Robotics transformer for real-world control at scale. *arXiv*, 2022.

[4] Anthony Brohan, Noah Brown, Justice Carbalal, Yevgen Chebotar, Xi Chen, Krzysztof Choromanski, Tianli Ding, Danny Driess, Avinava Dubey, Chelsea Finn, et al. Rt-2: Vision-language-action models transfer web knowledge to robotic control. *arXiv preprint arXiv:2307.15818*, 2023.

[5] Huayu Chen, Cheng Lu, Chengyang Ying, Hang Su, and Jun Zhu. Offline reinforcement learning via high-fidelity generative behavior modeling. *arXiv preprint arXiv:2209.14548*, 2022.

[6] Yinbo Chen and Xiaolong Wang. Transformers as meta-learners for implicit neural representations. In *Computer Vision–ECCV 2022: 17th European Conference, Tel Aviv, Israel, October 23–27, 2022, Proceedings, Part XVII*, pages 170–187. Springer, 2022.

[7] Yinbo Chen, Sifei Liu, and Xiaolong Wang. Learning continuous image representation with local implicit image function. In *Proceedings of the IEEE/CVF conference on computer vision and pattern recognition*, pages 8628–8638, 2021.

[8] Cheng Chi, Siyuan Feng, Yilun Du, Zhenjia Xu, Eric Cousineau, Benjamin Burchfiel, and Shuran Song. Diffusion policy: Visuomotor policy learning via action diffusion. *arXiv preprint arXiv:2303.04137*, 2023.

[9] Danny Driess, Ingmar Schubert, Pete Florence, Yunzhu Li, and Marc Toussaint. Reinforcement learning with neural radiance fields. *NeurIPS*, 2022.

[10] Philippe Hansen-Estruch, Ilya Kostrikov, Michael Janner, Jakub Grudzien Kuba, and Sergey Levine. Idql: Implicit q-learning as an actor-critic method with diffusion policies. *arXiv preprint arXiv:2304.10573*, 2023.

[11] Jonathan Ho, Ajay Jain, and Pieter Abbeel. Denoising diffusion probabilistic models. *Advances in neural information processing systems*, 33:6840–6851, 2020.

[12] Siyuan Huang, Zan Wang, Puha Li, Baoxiong Jia, Tengyu Liu, Yixin Zhu, Wei Liang, and Song-Chun Zhu. Diffusion-based generation, optimization, and planning in 3d scenes. In *Proceedings of the IEEE/CVF Conference on Computer Vision and Pattern Recognition*, pages 16750–16761, 2023.

[13] Andrew Jaegle, Felix Gimeno, Andy Brock, Oriol Vinyals, Andrew Zisserman, and Joao Carreira. Perceiver: General perception with iterative attention. In *ICML*, 2021.

[14] Stephen James, Zicong Ma, David Rovick Arrojo, and Andrew J Davison. Rlbench: The robot learning benchmark & learning environment. *RA-L*, 2020.

[15] Stephen James, Kentaro Wada, Tristan Laidlow, and Andrew J Davison. Coarse-to-fine q-attention: Efficient learning for visual robotic manipulation via discretisation. In *CVPR*, 2022.

[16] Eric Jang, Alex Irpan, Mohi Khansari, Daniel Kappler, Frederik Ebert, Corey Lynch, Sergey Levine, and Chelsea Finn. Bc-z: Zero-shot task generalization with robotic imitation learning. In *CoRL*, 2022.

[17] Wonbong Jang and Lourdes Agapito. Codenerf: Disentangled neural radiance fields for object categories. In *Proceedings of the IEEE/CVF International Conference on Computer Vision*, pages 12949–12958, 2021.

[18] Michael Janner, Yilun Du, Joshua B Tenenbaum, and Sergey Levine. Planning with diffusion for flexible behavior synthesis. *arXiv preprint arXiv:2205.09991*, 2022.

[19] Zhenyu Jiang, Yifeng Zhu, Maxwell Svetlik, Kuan Fang, and Yuke Zhu. Synergies between affordance and geometry: 6-dof grasp detection via implicit representations. *arXiv preprint arXiv:2104.01542*, 2021.

[20] Dmitry Kalashnikov, Alex Irpan, Peter Pastor, Julian Ibarz, Alexander Herzog, Eric Jang, Deirdre Quillen, Ethan Holly, Mrinal Kalakrishnan, Vincent Vanhoucke, et al. Qt-opt: Scalable deep reinforcement learning for vision-based robotic manipulation. *arXiv*, 2018.

[21] James J Kuffner and Steven M LaValle. Rrt-connect: An efficient approach to single-query path planning. In *Proceedings 2000 ICRA. Millennium Conference. IEEE International Conference on Robotics and Automation. Symposia Proceedings (Cat. No. 00CH37065)*, volume 2, pages 995–1001. IEEE, 2000.

[22] Yulong Li, Shubham Agrawal, Jen-Shuo Liu, Steven K Feiner, and Shuran Song. Scene editing as teleoperation: A case study in 6dof kit assembly. In *IROS*, 2022.

[23] Yunzhu Li, Shuang Li, Vincent Sitzmann, Pulkit Agrawal, and Antonio Torralba. 3d neural scene representations for visuomotor control. In *Conference on Robot Learning*, pages 112–123. PMLR, 2022.

[24] Zhixuan Liang, Yao Mu, Mingyu Ding, Fei Ni, Masayoshi Tomizuka, and Ping Luo. Adaptdiffuser: Diffusion models as adaptive self-evolving planners. *arXiv preprint arXiv:2302.01877*, 2023.

[25] Kai-En Lin, Yen-Chen Lin, Wei-Sheng Lai, Tsung-Yi Lin, Yi-Chang Shih, and Ravi Ramamoorthi. Vision transformer for nerf-based view synthesis from a single input image. In *Proceedings of the IEEE/CVF Winter Conference on Applications of Computer Vision*, pages 806–815, 2023.

[26] Yen-Chen Lin, Pete Florence, Andy Zeng, Jonathan T Barron, Yilun Du, Wei-Chiu Ma, Anthony Simeonov, Alberto Rodriguez Garcia, and Phillip Isola. Mira: Mental

imagery for robotic affordances. In *Conference on Robot Learning*, pages 1916–1927. PMLR, 2023.

[27] Lars Mescheder, Michael Oechsle, Michael Niemeyer, Sebastian Nowozin, and Andreas Geiger. Occupancy networks: Learning 3d reconstruction in function space. In *Proceedings of the IEEE/CVF conference on computer vision and pattern recognition*, pages 4460–4470, 2019.

[28] Ben Mildenhall, Pratul P Srinivasan, Matthew Tancik, Jonathan T Barron, Ravi Ramamoorthi, and Ren Ng. Nerf: Representing scenes as neural radiance fields for view synthesis. *Communications of the ACM*, 65(1):99–106, 2021.

[29] Arsalan Mousavian, Clemens Eppner, and Dieter Fox. 6-dof graspnet: Variational grasp generation for object manipulation. In *ICCV*, 2019.

[30] Adithyavairavan Murali, Arsalan Mousavian, Clemens Eppner, Chris Paxton, and Dieter Fox. 6-dof grasping for target-driven object manipulation in clutter. In *2020 IEEE International Conference on Robotics and Automation (ICRA)*, pages 6232–6238. IEEE, 2020.

[31] Michael Niemeyer, Lars Mescheder, Michael Oechsle, and Andreas Geiger. Occupancy flow: 4d reconstruction by learning particle dynamics. In *Proceedings of the IEEE/CVF international conference on computer vision*, pages 5379–5389, 2019.

[32] Maxime Oquab, Timothée Darcet, Théo Moutakanni, Huy Vo, Marc Szafraniec, Vasil Khalidov, Pierre Fernandez, Daniel Haziza, Francisco Massa, Alaaeldin El-Nouby, et al. Dinov2: Learning robust visual features without supervision. *arXiv preprint arXiv:2304.07193*, 2023.

[33] Jeong Joon Park, Peter Florence, Julian Straub, Richard Newcombe, and Steven Lovegrove. Deepsdf: Learning continuous signed distance functions for shape representation. In *Proceedings of the IEEE/CVF conference on computer vision and pattern recognition*, pages 165–174, 2019.

[34] Ethan Perez, Florian Strub, Harm De Vries, Vincent Dumoulin, and Aaron Courville. Film: Visual reasoning with a general conditioning layer. In *Proceedings of the AAAI conference on artificial intelligence*, 2018.

[35] Charles Ruizhongtai Qi, Li Yi, Hao Su, and Leonidas J Guibas. Pointnet++: Deep hierarchical feature learning on point sets in a metric space. *Advances in neural information processing systems*, 30, 2017.

[36] Guocheng Qian, Yuchen Li, Houwen Peng, Jinjie Mai, Hasan Hammoud, Mohamed Elhoseiny, and Bernard Ghanem. Pointnext: Revisiting pointnet++ with improved training and scaling strategies. *Advances in Neural Information Processing Systems*, 35:23192–23204, 2022.

[37] Alec Radford, Jong Wook Kim, Chris Hallacy, Aditya Ramesh, Gabriel Goh, Sandhini Agarwal, Girish Sastry, Amanda Askell, Pamela Mishkin, Jack Clark, et al. Learning transferable visual models from natural language supervision. In *ICML*, 2021.

[38] Rouhollah Rahmatizadeh, Pooya Abolghasemi, Ladislau Böloni, and Sergey Levine. Vision-based multi-task manipulation for inexpensive robots using end-to-end learning from demonstration. In *2018 IEEE international conference on robotics and automation (ICRA)*, pages 3758–3765. IEEE, 2018.

[39] Jeremy Reizenstein, Roman Shapovalov, Philipp Henzler, Luca Sbordone, Patrick Labatut, and David Novotny. Common objects in 3d: Large-scale learning and evaluation of real-life 3d category reconstruction. In *Proceedings of the IEEE/CVF International Conference on Computer Vision*, pages 10901–10911, 2021.

[40] Konstantinos Rematas, Ricardo Martin-Brualla, and Vittorio Ferrari. Sharf: Shape-conditioned radiance fields from a single view. *arXiv preprint arXiv:2102.08860*, 2021.

[41] Dongseok Shim, Seungjae Lee, and H Jin Kim. Snerl: Semantic-aware neural radiance fields for reinforcement learning. *ICML*, 2023.

[42] Mohit Shridhar, Lucas Manuelli, and Dieter Fox. Cliprot: What and where pathways for robotic manipulation. In *CoRL*, 2022.

[43] Mohit Shridhar, Lucas Manuelli, and Dieter Fox. Perceiver-actor: A multi-task transformer for robotic manipulation. In *CoRL*, 2023.

[44] Mohit Shridhar, Lucas Manuelli, and Dieter Fox. Perceiver-actor: A multi-task transformer for robotic manipulation. In *Conference on Robot Learning*, pages 785–799. PMLR, 2023.

[45] Vincent Sitzmann, Michael Zollhöfer, and Gordon Wetzstein. Scene representation networks: Continuous 3d-structure-aware neural scene representations. *Advances in Neural Information Processing Systems*, 32, 2019.

[46] Jascha Sohl-Dickstein, Eric Weiss, Niru Maheswaranathan, and Surya Ganguli. Deep unsupervised learning using nonequilibrium thermodynamics. In *International conference on machine learning*, pages 2256–2265. PMLR, 2015.

[47] Shuran Song, Andy Zeng, Johnny Lee, and Thomas Funkhouser. Grasping in the wild: Learning 6dof closed-loop grasping from low-cost demonstrations. *IEEE Robotics and Automation Letters*, 5(3):4978–4985, 2020.

[48] Alex Trevithick and Bo Yang. Grf: Learning a general radiance field for 3d representation and rendering. In *Proceedings of the IEEE/CVF International Conference on Computer Vision*, pages 15182–15192, 2021.

[49] Julen Urain, Niklas Funk, Georgia Chalvatzaki, and Jan Peters. Se (3)-diffusionfields: Learning cost functions for joint grasp and motion optimization through diffusion. *arXiv preprint arXiv:2209.03855*, 2022.

[50] Qianqian Wang, Zhicheng Wang, Kyle Genova, Pratul P Srinivasan, Howard Zhou, Jonathan T Barron, Ricardo Martin-Brualla, Noah Snavely, and Thomas Funkhouser. Ibrnet: Learning multi-view image-based rendering. In *Proceedings of the IEEE/CVF Conference on Computer Vision and Pattern Recognition*, pages 4690–4699, 2021.

[51] Zhendong Wang, Jonathan J Hunt, and Mingyuan Zhou. Diffusion policies as an expressive policy class for offline reinforcement learning. *arXiv preprint arXiv:2208.06193*, 2022.

2022.

- [52] Jianxiong Xiao, Andrew Owens, and Antonio Torralba. Sun3d: A database of big spaces reconstructed using sfm and object labels. In *Proceedings of the IEEE international conference on computer vision*, pages 1625–1632, 2013.
- [53] Zhenjia Xu, Zhanpeng He, and Shuran Song. Universal manipulation policy network for articulated objects. *RA-L*, 2022.
- [54] Ruihan Yang, Huazhe Xu, Yi Wu, and Xiaolong Wang. Multi-task reinforcement learning with soft modularization. *Advances in Neural Information Processing Systems*, 33:4767–4777, 2020.
- [55] Tianhe Yu, Deirdre Quillen, Zhanpeng He, Ryan Julian, Karol Hausman, Chelsea Finn, and Sergey Levine. Metaworld: A benchmark and evaluation for multi-task and meta reinforcement learning. In *Conference on robot learning*, pages 1094–1100. PMLR, 2020.
- [56] Yanjie Ze, Nicklas Hansen, Yinbo Chen, Mohit Jain, and Xiaolong Wang. Visual reinforcement learning with self-supervised 3d representations. *RA-L*, 2023.
- [57] Yanjie Ze, Ge Yan, Yueh-Hua Wu, Annabella Macaluso, Yuying Ge, Jianglong Ye, Nicklas Hansen, Li Erran Li, and Xiaolong Wang. Gnfactor: Multi-task real robot learning with generalizable neural feature fields. *arXiv preprint arXiv:2308.16891*, 2023.

APPENDIX

To enhance the reproducibility of DNAct, we summarize the experiment details such as the configurations and parameters used in Table VI.

TABLE VI: Hper-parameters. We list all hyper-parameters for reproducing DNAct results below.

Parameter	Value
training iteration	50K
Learning rate Scheduler	False
Optimizer	Adam
learning rate	0.0005
Weight Decay	1×10^{-6}
Translation loss coefficient (λ_{trans})	300
Rotation loss coefficient (λ_{trans})	1
Gripper openness loss coefficient (λ_{trans})	1
Collision loss coefficient (λ_{trans})	1
Diffusion loss coefficient (λ_{diff})	5
denoising steps (training)	100
ray batch size b_{ray}	512
embedding loss coefficient λ_{feat}	0.01
Batch size	32
GPU	RTX 3090

We have chosen ten language-conditioned tasks from RL-Bench [14]. An overview of these tasks is presented in Table VII. Our variations include randomly sampled colors, sizes, placements, and object categories. The color set includes twenty instances: red, maroon, lime, green, blue, navy, yellow, cyan, magenta, silver, gray, orange, olive, purple, teal, azure, violet, rose, black, and white. The size set comprises two types: short and tall. The placements and object categories are specific to each task. The average keyframes numbers are varied from 2 to 15, representing different horizon length.

We demonstrate the keyframes from two of our real robot tasks.

3D Encoder. We use a 3D UNet with 4.72M parameters to encode the input voxel $100^3 \times 10$ into a deep 3D volumetric representation of size $100^3 \times 64$. We provide the PyTorch-Style pseudo-code for the forward process as follows. Each conv layer comprises a single 3D Convolutional Layer, followed by Batch Normalization, and Leaky ReLU activation.

```
def forward(self, x):
    conv0 = self.conv0(x) # 100^3x8
    conv2 = self.conv2(self.conv1(conv0)) #
    ↪ 50^3x16
    conv4 = self.conv4(self.conv3(conv2)) #
    ↪ 25^3x32
    conv6 = self.conv6(self.conv5(conv4)) #
    ↪ 13^3x64
    conv8 = self.conv8(self.conv7(conv6)) # 7^3
    ↪ x128
    x = self.conv10(self.conv9(conv8)) # 7^3
    ↪ x256
    x = conv8 + self.conv11(x) # 7^3x128
    x = conv6 + self.conv13(x) # 13^3x64
    x = conv4 + self.conv15(x) # 25^3x32
```

```
x = conv2 + self.conv17(x) # 50^3x16
x = self.conv_out(conv0 + self.conv19(x)) #
↪ 100^3x64
return x
```

Fusion Decoder. We use several set abstraction blocks to fuse pre-trained 3D semantics feature, geometric point cloud feature, language feature from CLIP and robot proprioception embedding. This generates a vision-language feature of size 1024 as input of policy MLP.

Noise Predictor. The architecture of the noise predictor is a modified U-Net architecture designed to handle 1D inputs and incorporates conditional inputs. It's comprised of an Encoder, Decoder, and additional components to process conditional inputs.

- **Encoder:** The encoder is composed of a sequence of conditional residual block and each block has two “Conv1d → GroupNorm → Mish” components. A downsampling layer is applied after each block, performing downsampling with Conv1d.
- **Decoder:** Similar to the encoder while replacing the downsampling layers with upsampling layers performed by ConvTranspose1d.
- **Final Convolution Layer:** A sequence comprising a “Conv1d → GroupNorm → Mish” and Conv1d layer.

We apply the Feature-wise Linear Modulation (FiLM) [34] to enable the noise predictor to predict the noise with conditional input, the fused feature. This technique is particularly useful in conditional generation tasks. The FiLM module performs modulation by applying a simple affine transformation to each feature map. Given a feature map x , the FiLM transformation is defined as:

$$\text{FiLM}(x) = \gamma \cdot x + \beta, \quad (7)$$

where x is the input feature map, γ is the scale parameter, and β is the shift parameter. In our noise predictor architecture, the fused feature is used to predict the FiLM parameters γ and β . The predicted parameters are then used to modulate the feature maps within each block.

Policy MLP. The Policy MLP is composed of several MLPs. The translation output has one independent MLP and the remaining rotation, collision, and open action, share another set of MLP.

TABLE VII: **Language-conditioned tasks in RLBench [14].**

Task	Variation Type	# of Variations	Avg. Keyframes	Language Template
turn tap	placement	2	2.0	“turn — tap”
drag stick	color	20	6.0	“use the stick to drag the cube onto the — — target”
open fridge	placement	1	4.4	“open the fridge door”
put in drawer	placement	3	15.0	“put the item in the — drawer”
sweep to dustpan	size	2	4.6	“sweep dirt to the — dustpan”
meat off grill	category	2	5.0	“take the — off the grill”
phone on base	placement	1	6.4	“put the phone on the base”
place wine	placement	3	6.2	“stack the wine bottle to the — of the rack”
slide block	color	4	4.7	“slide the block to — target”
put in safe	placement	3	6.1	“put the money away in the safe on the — shelf”

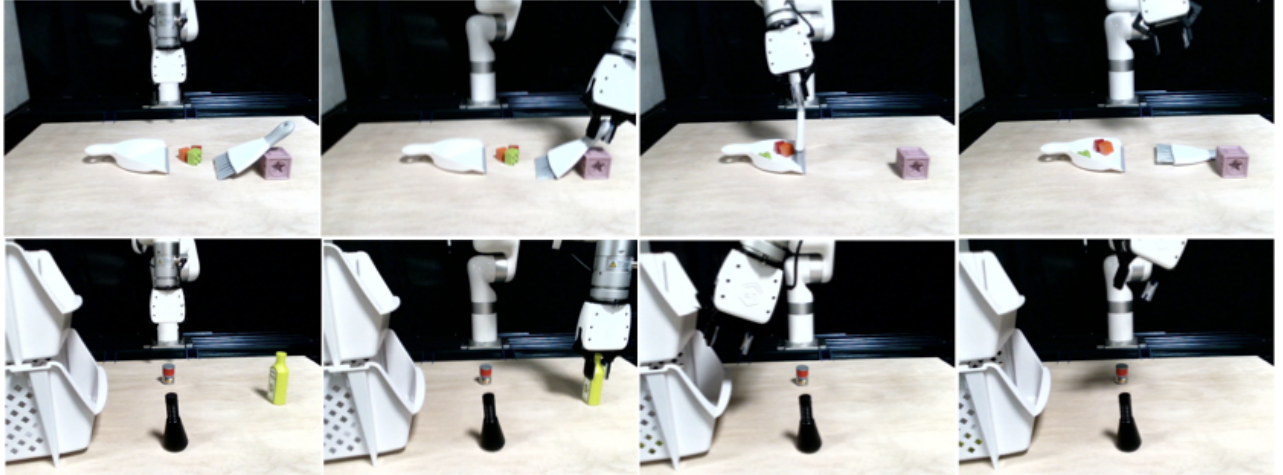


Fig. 8: **Keyframes for Real-Robot tasks** We give two examples of keyframes used in our real robot tasks.

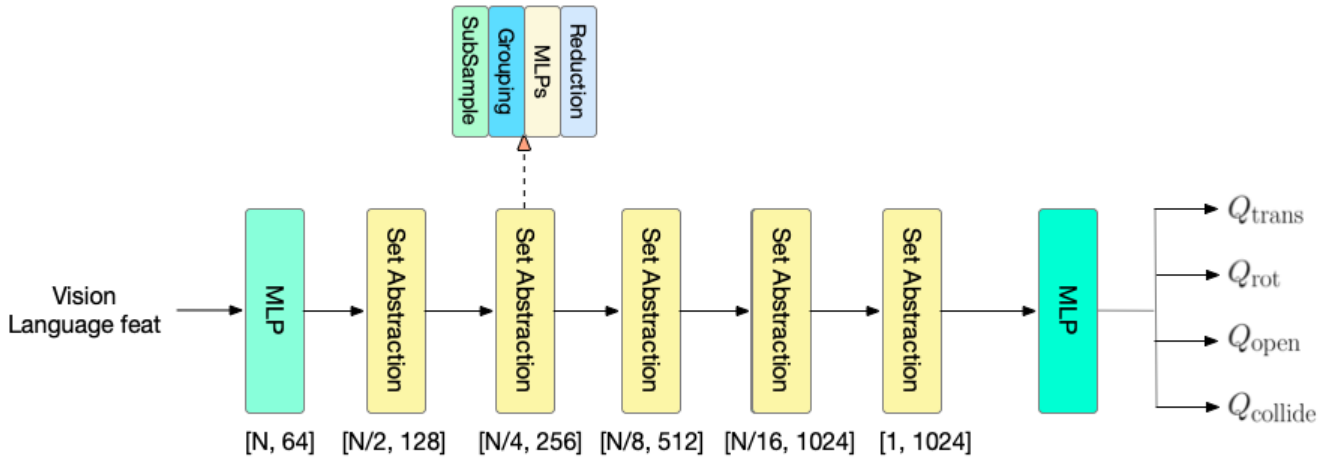


Fig. 9: **Fusion Decoder Architecture.**